COMMUNICATION

Check for updates

Differential intracellular influence of cancer cells and normal cells on magnetothermal properties and magnetic hyperthermal effects of magnetic nanoparticles†

Man Wang,[ab] Rui Sun,[ab] Huajian Chen, [ID][a] Toru Yoshitomi, [ID][a] Hiroaki Mamiya,[c] Masaki Takeguchi, [ID][d] Naoki Kawazoe,[a] Yingnan Yang[e] and Guoping Chen [ID]*[ab]

Magnetic hyperthermia using heat locally generated by magnetic nanoparticles (MNPs) under an alternating magnetic field (AMF) to ablate cancer cells has attracted enormous attention. The high accumulation of MNPs and slow heat dissipation generated in tumors are considered the dominant factors involved in magnetic hyperthermia. However, the influence of intracellular microenvironment on magnetic hyperthermia has been ignored. This study unveiled for the first time the critical role of intracellular microenvironment on magnetic hyperthermia. The intracellular microenvironments of cancer cells and normal cells showed different influence on the magnetothermal properties and magnetic hyperthermia effects of MNPs. The MNPs in cancer cells could generate higher temperatures and induce higher rates of apoptosis than those in normal cells. Compared with that of normal cells, the intracellular microenvironment of cancer cells was more conducive to Brownian relaxation and the dynamic magnetic response of internalized MNPs. The cancerous intracellular microenvironment had a discriminative effect on the magnetic hyperthermal effect of MNPs due to the low viscoelasticity of cancer cells, which was verified by the softening or stiffening of cells and simulation models created using viscous liquids or elastic hydrogels. These findings suggest that the intracellular microenvironment should be considered another critical factor of the magnetic hyperthermal effect of MNPs.

New concepts

Our study unveils the critical role of intracellular microenvironment of cancer cells in magnetic hyperthermia. The intracellular microenvironment of cancer cells is more conducive to the magnetothermal conversion and magnetic hyperthermal effect of MNPs than the normal healthy cells. The internalized MNPs in cancer cells can generate higher temperatures and induce higher rates of apoptosis than the MNPs in normal cells. The intracellular microenvironment of cancer cells has been demonstrated one of the dominant factors of magnetic hyperthermia.

Introduction

Magnetic hyperthermia, which involves the use of magnetic nanoparticles (MNPs) to generate localized heat under an alternating magnetic field (AMF) of appropriate field intensity (few tens of kA m^{-1}) and frequency range (100–300 kHz),[1–3] has been developed as a promising approach for cancer treatment because of its tissue penetration depth[4–6] and biocompatibility.[7,8] The use of magnetic hyperthermia to treat prostate cancer and pancreatic cancer has been approved by the U.S. Food and Drug Administration.[9] Numerous clinical trials have been conducted by MagForce AG (Berlin, Germany) to investigate the efficacy of magnetic hyperthermia for the treatment of pancreatic cancer.[5,9] However, magnetic hyperthermia can not only ablate cancer cells but also affect normal healthy cells because cancer cells and normal cells coexist within the same milieu,[10] and all these cells can take up MNPs.[11–13] Understanding the principles of magnetic hyperthermia and its cellular bias is critical to maximize its anticancer therapeutic effect while minimizing its negative side effects on normal healthy cells.

The different vasculatures of tumors and healthy tissues are generally considered to contribute to the success of magnetic hyperthermia. Healthy tissues have an orderly and efficient vascular network and lymphatic vessels for blood circulation and lymphatic drainage. However, tumors have disorganized

[a] Research Center for Macromolecules and Biomaterials, National Institute for Materials Science, Ibaraki 305-0044, Japan. E-mail: Guoping.CHEN@nims.go.jp

[b] Graduate School of Science and Technology, University of Tsukuba, Ibaraki 305-8577, Japan

[c] Research Center for Magnetic and Spintronic Materials, National Institute for Materials Science, Ibaraki 305-0047, Japan

[d] Research Center for Energy and Environmental Materials, National Institute for Materials Science, Ibaraki 305-0047, Japan

[e] Graduate School of Life and Environmental Science, University of Tsukuba, Ibaraki 305-8572, Japan

† Electronic supplementary information (ESI) available. See DOI: https://doi.org/10.1039/d5mh00317b

and chaotic vascular networks and lymphatic vessels that are immature, tortuous, and hyperpermeable.[14,15] The hyperpermeable vasculature and poor lymphatic drainage allow the MNPs to extravasate from the vasculature and remain in the tumors, thereby enhancing the cellular uptake of MNPs by cancer cells, which is known as the enhanced permeability and retention (EPR) effect.[16] The increased uptake and retention of MNPs in cancer cells results in the generation of high local temperatures to effectively ablate cancer cells. Moreover, the distorted vasculature cannot dissipate heat easily, resulting in the overheating of tumors.

In addition to the effects of the typical characteristics of the vasculature of tumors, other factors affecting the magnetothermal properties of MNPs should also be considered.[17–19] The microenvironment surrounding MNPs can affect the Brownian relaxation of superparamagnetic MNPs and their magnetothermal conversion.[20–22] Nevertheless, it is unclear whether the intracellular microenvironment of different cell types affects the magnetothermal properties of MNPs or if the cells themselves can discriminate magnetic hyperthermia. Therefore, the aim of this study was to investigate how the intracellular environment of cancer cells and normal cells affects the magnetothermal properties and magnetic hyperthermal effect of MNPs. Human bone osteosarcoma cells (MG63 cells), normal human osteoblasts (NHOst cells) and human bone marrow-derived mesenchymal stem cells (MSCs), which are related to bone osteosarcoma,[23] were used to compare whether different cell types affect the magnetothermal properties of MNPs and their magnetic hyperthermia efficiency (Scheme 1). The results indicated that the intracellular environment of cancer cells was discriminatively beneficial for the magnetothermal conversion and magnetic

hyperthermal effect of MNPs, which could be another key factor of magnetic hyperthermia.

Results

Characterization and cellular interaction of MNPs

The MNPs were synthesized and modified with citrate for colloidal stability in culture medium.[24] The MNPs had a flower-like shape with an average size of 30.2 ± 4.9 nm (Fig. 1(A) and (B)). X-ray Diffraction (XRD) demonstrated that each diffraction peak of the bare-MNPs and citrate-MNPs corresponded to the standard Fe_3O_4 pattern (JCPDS file no. 19-0629) and the lack of additional peaks indicated that the synthesized MNPs were composed of pure-phase Fe_3O_4 with a cubic spinel structure (Fig. 1(C)).[25] The surface chemical state of the bare-MNPs and citrate-MNPs was analyzed by X-ray photoelectron spectroscopy (XPS).[26] The Fe 2p spectra of the bare-MNPs (ESI,† Fig. S1A) and citrate-MNPs (Fig. 1(D)) exhibited two primary peaks at ~710 eV and ~723 eV, corresponding to Fe $2p_{3/2}$ and Fe $2p_{1/2}$, respectively, which are characteristic of Fe_3O_4.[27] XPS profiles of O1s electrons of the bare MNPs (ESI,† Fig. S1B) and citrate MNPs (Fig. 1(E)) were deconvoluted into two peaks located at ~529 eV and ~531 eV, corresponding to the oxygen in O–H or O–C components and oxygen species in the Fe–O component of magnetite, respectively. The C 1s spectra provided insight into the presence of citrate on the Fe_3O_4 surface. Analysis of the citrate-MNPs spectrum C 1s region (Fig. 1(F)) revealed an enlarged C=O peak area (25.2%) in comparison to that of the bare-MNPs spectrum (18.6%) (ESI,† Fig. S1C). Modification of the MNPs by citrate was further confirmed by Fourier
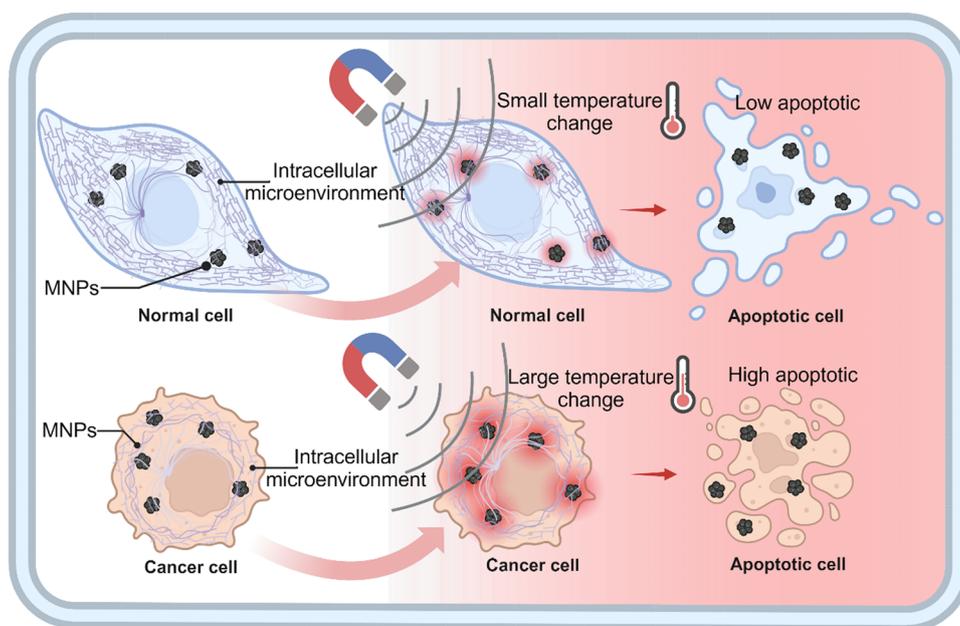
Scheme 1 Differential influence of the intracellular microenvironment of cancer cells and normal cells on the magnetothermal properties of internalized MNPs and the magnetic hyperthermia efficiency. The illustration was generated with BioRender (https://app.biorender.com/).
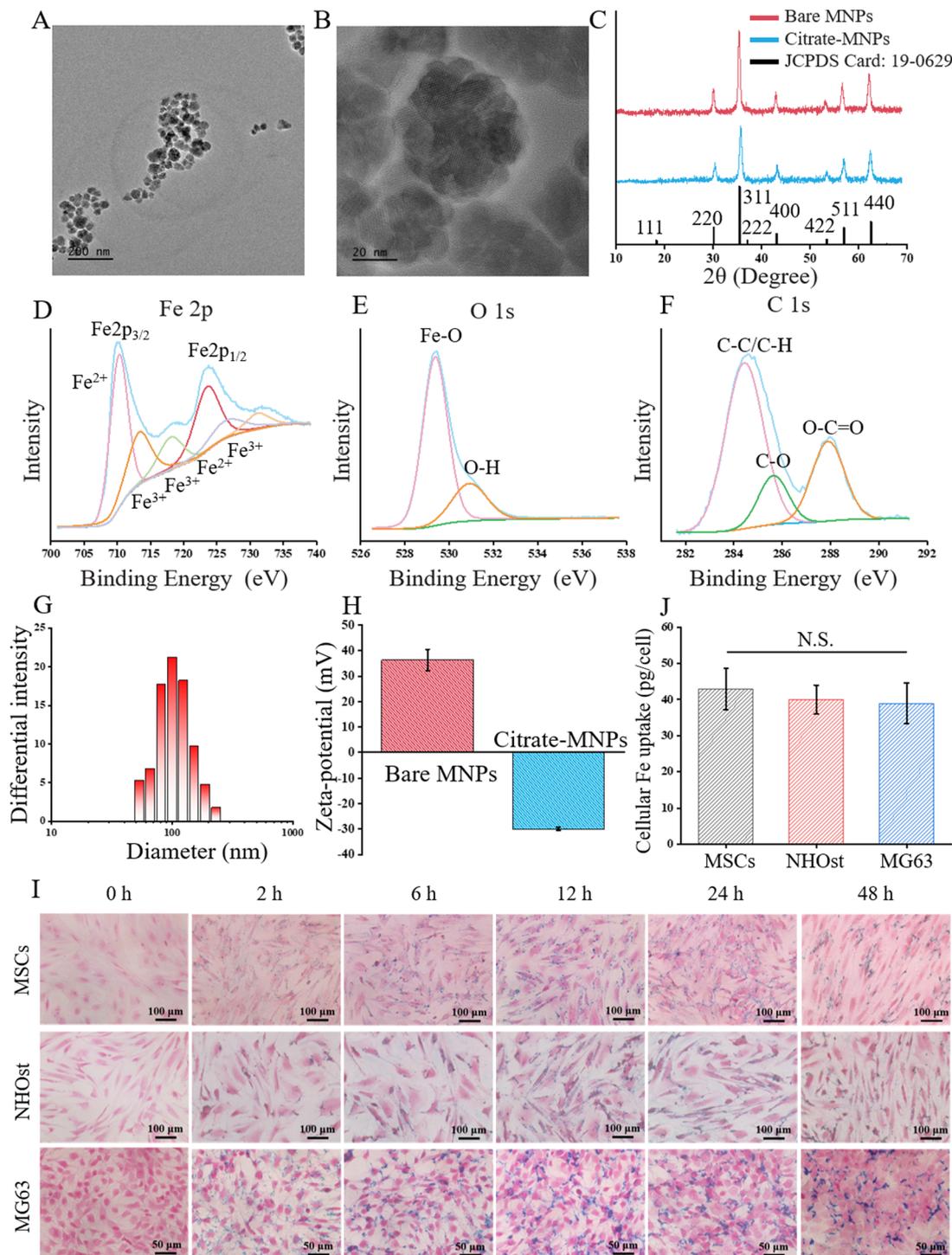
Fig. 1 Physical characterization and cellular uptake of MNPs. TEM images of MNPs at (A) low and (B) high magnification. (C) XRD patterns of bare-MNPs, citrate-MNPs and JCPDS card: 19-0629. XPS analysis and fitted curves of (D) Fe 2p peaks, (E) O 1s peaks and (F) C 1s peaks of citrate-MNPs. (G) Hydrodynamic size distribution of citrate-MNPs. (H) Zeta potentials of bare-MNPs and citrate-MNPs. (I) Prussian blue staining of MNPs in MSCs, NHOst cells and MG63 cells after culture with 120 $\mu g\ mL^{-1}$ MNPs for 0, 2, 6, 12, 24 and 48 h. (J) Cellular uptake of MNPs by MSCs, NHOst cells and MG63 cells after culture with 120 $\mu g\ mL^{-1}$ MNPs for 12 h. Data are expressed as the mean $\pm$ S.D. (n = 3). N.S.: no significant difference.

transform infrared spectroscopy (FT-IR), which revealed characteristic absorption peaks of COO^- groups at 1388.7 and 1568.1 cm^{-1} (ref. 25) (ESI,† Fig. S1D).

The citrate-MNPs exhibited superparamagnetic properties at room temperature (ESI,† Fig. S1E). The citrate-MNPs could be well dispersed in aqueous solution without precipitation (ESI,† Fig. S1F).

The hydrodynamic size of citrate-MNPs in water (Fig. 1(G)), MSC growth medium (MSCGM), osteoblast basal medium (OBM) and Dulbecco's modified Eagle's medium with high glucose (DMEM) was 106.7 ± 37.3, 118.6 ± 42.5, 128.7 ± 36.7 and 133.0 ± 46.4 nm, respectively (ESI,† Fig. S1G–I). The hydrodynamic diameters of the citrate-MNPs in water and media were not significantly different, indicating good colloidal stability of the MNPs in the physiological environment. The zeta potential of the bare-MNPs was 36.3 ± 4.2 mV (Fig. 1(H)). After modification, the zeta potential of the citrate-MNPs was -29.9 ± 0.5 mV owing to the introduction of citrate groups on the MNPs surface. The citrate-MNPs were used in all the following experiments.

The MNPs were subsequently used for cell culture to investigate their optimal concentration for magnetic hyperthermia. Without AMF exposure, the MNPs cannot generate heat, and the influence of MNPs on cell viability without AMF exposure was first evaluated. Three types of osteosarcoma microenvironment-related cells (MG63 cells, NHOst cells and MSCs) were cultured with MNPs at concentrations ranging from 0 to 240 μg mL^{-1}. Live/dead staining revealed that the MNPs did not affect cell viability at concentrations ranging from 0 to 120 μg mL^{-1}, as all the cells were alive (ESI,† Fig. S2A, C and E). When the concentration of MNPs increased to 240 μg mL^{-1}, some dead cells (red fluorescence) were observed. The quantification of cell viability via the WST-1 assay also demonstrated that cell viability was not significantly affected by MNPs concentrations up to 120 μg mL^{-1} (ESI,† Fig. S2B, D and F). A high concentration of MNPs (240 μg mL^{-1}) significantly reduced cell viability. The cell morphology did not change when the cells were cultured with 120 μg mL^{-1} MNPs for 12 h (ESI,† Fig. S3). These results indicated that MNPs up to 120 μg mL^{-1} were compatible with all the cells. Therefore, MNPs at a concentration of 120 μg mL^{-1} were used in the following experiments.

The cellular uptake of the MNPs was monitored during cell culture. MSCs, NHOst cells and MG63 cells were cultured with 120 μg mL^{-1} MNPs for 0–48 h, and Prussian blue staining was used to visualize the internalized MNPs (Fig. 1(I)). When the cells were cultured with MNPs, MNPs were detected in all the cells. The three types of cells showed similar uptake performance. The cellular uptake of MNPs increased with culture time within 12 h. However, prolonged culture duration beyond 12 h led to a reduction in internalized MNPs, which was attributable to cell proliferation and metabolic processes. ICP-OES quantification revealed that the amount of MNPs internalized by MSCs, NHOst cells and MG63 cells after 12 h of culture was 41.9 ± 5.7, 40.0 ± 4.0 and 38.9 ± 5.7 pg per cell, respectively. The cellular uptake amount of MNPs among the three types of cells was almost the same (Fig. 1(J)). Accordingly, the subsequent experiments were performed with an MNP concentration of 120 μg mL^{-1} and a cell culture time of 12 h to achieve maximal cellular uptake of MNPs with minimal influence on cell viability.

Influence of the intracellular microenvironment of cancer cells and normal cells on the magnetothermal properties of MNPs

To investigate whether the intracellular microenvironment of different cell types affects the magnetothermal properties of MNPs, cancer cells (MG63) and normal cells (MSCs and NHOst cells) were cultured with 120 μg mL^{-1} MNPs for 12 h. After 12 h of culture with MNPs, the cells were washed, collected and exposed to an AMF. The temperature change was recorded, and the specific absorption rate (SAR), an indicator of the magnetothermal conversion efficiency, was calculated. As shown in Fig. 2(A), the temperature of the three types of cells increased with increasing AMF irradiation time. However, the temperature increase in cancer cells (MG63 cells) was significantly greater than that in normal cells (MSCs and NHOst cells). The SAR of cancer cells was also significantly greater than that of normal cells (Fig. 2(E)). The results indicated that the intracellular microenvironment of cancer cells and normal cells had different effects on magnetothermal conversion efficiency and that compared with normal cells, cancer cells facilitated the magnetothermal conversion of MNPs.

The favorability of the cancerous intracellular microenvironment for the magnetothermal conversion of MNPs might be due to the disordered cytoskeletal structure of cancer cells. It has been reported that cancer cells have disordered cytoskeletons and are softer than their normal counterpart cells.[23,28–31] Actin filament staining indicated that normal cells (MSCs and NHOst cells) presented well-organized actin filaments across cell bodies, whereas cancer cells presented disordered actin filament organization with predominant assembly in peripheral regions (ESI,† Fig. S4A). The uptake of MNPs did not affect actin filament organization in either normal cells or cancer cells (ESI,† Fig. S4B).

To demonstrate the influence of the cytoskeleton on the magnetothermal conversion of MNPs, softening and stiffening of the cells by cytochalasin D (Cyto D) and paraformaldehyde (PFA) fixation were conducted, and the treated cells were used for magnetothermal conversion evaluation. The actin filaments of both normal cells and cancer cells after Cyto D treatment showed similar disordered actin filament organization (ESI,† Fig. S4C and D). The internalized MNPs remained in the cells even after Cyto D treatment (ESI,† Fig. S4E and F). The magnetothermal conversion of the MNPs was compared after Cyto D, PFA fixation or lysis (ESI,† Fig. S5). All groups showed a gradual increase in temperature with increasing AMF irradiation time. The magnitude of the temperature increase differed among the different treatments. The lysed cells presented the fastest temperature increase and highest SAR, followed by the Cyto D-treated cells, intact cells and fixed cells, which corresponded with the cytoskeletal structure. Disturbance of the cytoskeleton increased the magnetothermal conversion efficiency, whereas fixation resulted in decreased efficiency of magnetothermal conversion of the MNPs.

When the cancer cells and normal cells were compared after lysis, Cyto D treatment and fixation, the cancer cells still presented greater increases in temperature and the SAR than the normal cells after Cyto D treatment (Fig. 2(B) and (E)). This occurred because the Cyto D treatment disturbed but did not destroy the cytoskeletal structure (ESI,† Fig. S4C and D). However, all the fixed and lysed cells presented the same temperature increase (Fig. 2(C) and (D)) and the same SAR
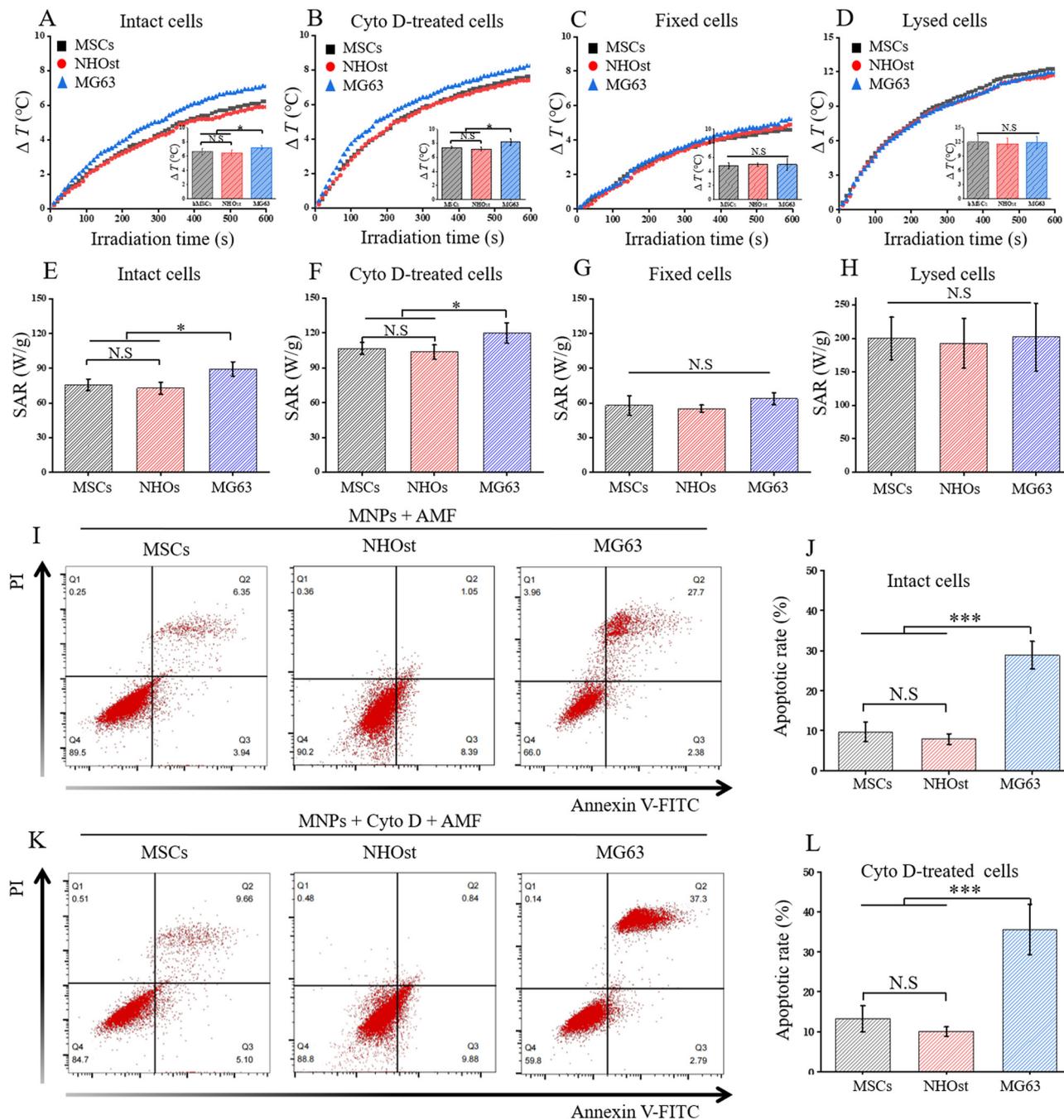
Fig. 2 Magnetothermal conversion (temperature change and SAR) and magnetic hyperthermal effect of intracellular MNPs in MSCs, NHOst cells and MG63 cells without any treatment or after Cyto D treatment, fixation or lysis. (A)–(D) Temperature-time curve during 10 min of AMF irradiation, temperature increase after 10 min of AMF irradiation, and (E)–(H) SAR of MNPs in (A), (E) intact cells, (B), (F) Cyto D-treated cells, (C), (G) fixed cells and (D), (H) lysed cells. (I), (K) Representative flow cytometry image of cell apoptosis and (J), (L) the apoptosis rates of (I), (J) intact cells and (K), (L) Cyto D-treated cells. Data are expressed as the mean $\pm$ S.D. ($n = 3$). Significant difference: *$p < 0.05$, ***$p < 0.001$. N.S.: no significant difference.

(Fig. 2(G) and (H)). This occurred because lysis released the MNPs from the cells, and the free MNPs had the same magnetothermal properties. Fixation crosslinked the cytoskeletal network and made the cells stiffer, which also resulted in the same magnetothermal properties of the MNPs in the fixed cells.

The results indicated that the intracellular MNPs in MG63 cells presented a significantly greater magnetothermal conversion efficiency and induced greater temperature changes than did the intracellular MNPs in normal cells because of the differences in cytoskeletal structure. A temperature just a few degrees above the physiological temperature can cause protein unfolding, entanglement, nonspecific aggregation, initiation of the heat shock response and ultimately induction of cell apoptosis.[32,33] The different temperature increases generated by the intracellular

MNPs in different cell types might induce different degrees of cell apoptosis. Cell apoptosis after AMF irradiation was evaluated *via* flow cytometry (Fig. 2(I)–(L) and ESI,† Fig. S6). The cells without MNPs were used as controls. Compared with the control group, there was no significant difference in the apoptosis rate of cells exposed to AMF alone, MNPs alone, or Cyto D alone, indicating that AMF irradiation, MNPs and Cyto D treatment did not induce cell apoptosis (ESI,† Fig. S6). In contrast, the apoptosis rate of cells in the MNP + AMF group increased significantly, which was attributed to the heat generated by the MNPs internalized within the cells. Furthermore, the cells in the MNP + Cyto D + AMF group had a greater apoptosis rate than did those in the MNP + AMF group; this occurred because Cyto D increased the magnetothermal conversion efficiency.

Interestingly, the cancer cells showed a greater apoptosis rate than did the normal cells when the different types of cells were compared (Fig. 2(I)–(L)). The MG63 cells in the MNP + AMF group exhibited a greater apoptosis rate than did those in the MSC and NHOst cell groups did, which can be explained by the greater magnetothermal conversion efficiency of the intracellular MNPs in the cancer cells. After Cyto D treatment, MG63 cells also presented a greater apoptosis rate than did MSCs and NHOst cells in the MNP + Cyto D + AMF group; this occurred because Cyto D treatment increased the magnetothermal conversion efficiency of intracellular MNPs, and the efficiency was greater in Cyto D-treated cancer cells than Cyto D-treated normal cells.

Discriminative magnetic hyperthermia of cancer cells *via* MNPs

To examine whether the magnetic hyperthermal effect of MNPs could discriminatively ablate cancer cells in a mixture of cancer cells and normal cells, cancer cells and normal cells were cocultured, and the magnetic hyperthermia induced by MNPs in different cell types was compared. The MG63 cells were labeled with green fluorescence protein (GFP) and then cocultured with normal cells (MSCs or NHOst cells). The cocultured cells were incubated with 120 μg mL^{-1} MNPs for 12 h. Then, the cells were washed, collected and exposed to AMF. The apoptosis rates of cancer cells and normal cells were compared (Fig. 3).

In the absence of MNPs (control), the apoptosis rate was very low, and there was no significant difference between cancer cells and normal cells, confirming that the AMF did not discriminatively affect the death of either cancer cells or normal cells. In the MNP + AMF group, the apoptosis rate of both cancer cells and normal cells increased due to the heat generated by the MNPs under the AMF. However, the apoptosis rate of cancer cells was significantly greater than that of normal cells. When MG63-GFP cells were cocultured with MSCs in the MNP + AMF group, the apoptosis rate of MG63-GFP cells (27.2 $\pm$ 1.4%) was significantly greater than that of MSCs (12.0 $\pm$ 2.0%) (Fig. 3(A) and (B)). When MG63-GFP cells were cocultured with NHOst cells in the MNP + AMF group, the apoptosis rate of MG63-GFP cells (25.5 $\pm$ 4.4%) was significantly greater than that of NHOst cells (10.9 $\pm$ 1.3%) (Fig. 3(C) and (D)). The results suggested that the magnetic hyperthermal effect of the MNPs could discriminatively induce more significant apoptosis in cancer cells than in normal cells in the mixed cell population. Until now, the enhanced cellular uptake of MNPs and poor heat dissipation have been considered the predominant factors related to the magnetic hyperthermal effect of MNPs. In addition to these factors, the intracellular microenvironment of cancer cells should be considered another critical factor.

Alternating current susceptibility of MNPs in different types of cells

The alternating current (AC) susceptibility of MNPs in different types of cells was measured to further explain the different influences of the intracellular microenvironment of cancer cells and normal cells on the magnetothermal conversion efficiency of MNPs. The AC susceptibility of free MNPs (MNPs dispersed in distilled water) is shown in Fig. 4(A). The real AC susceptibility component (χ') of free MNPs from 10 Hz to 10 kHz progressively decreased with increasing frequency. The imaginary component (χ'') showed a Brownian relaxation-related peak near 10 kHz, revealing the prevalence of Brownian relaxation of the synthesized MNPs with diameter around 30 nm in the studied frequency range.[9] This is consistent with the AC susceptibility of other previously reported superparamagnetic nanoparticles whose internal magnetic moment remains aligned with the AC field primarily through Brownian rotation during the AC field cycle.[20,34,35]

The AC susceptibility of MNPs in MSCs, NHOst cells and MG63 cells without treatment or after Cyto D treatment, PFA fixation or cell lysis was shown in Fig. 4(B)–(E) and ESI,† Fig. S7. The dynamic magnetic response of the intracellular MNPs, with the exception of those in the lysed cell group, clearly differed from that of MNPs in water. Compared with the AC susceptibility of free MNPs in water, the absolute value of χ'' of intracellular MNPs in all the cell types decreased across the entire frequency range (ESI,† Fig. S7), indicating the shifting of the Brownian relaxation peak to a lower frequency. Compared with that of the intracellular MNPs in intact cells, the χ'' value increased and the χ'' peak tended to shift toward a higher frequence after Cyto D treatment but the χ'' value decreased and the χ'' peak tended to shift toward a lower frequence after fixation. This trend was observed in all three types of cells, indicating that Cyto D treatment and fixation influenced the dynamic magnetic response of the intracellular MNPs by softening and stiffening the intracellular environment, respectively.

When the three types of cells were compared, the χ'' of MNPs within MG63 cells was greater than that of MNPs within MSCs and NHOst cells. The χ'' peak tended to shift toward a higher frequence than did that of the normal cells, indicating that the MNPs in the cancer cells had a greater dynamic magnetic response than did those in the normal cells (Fig. 4(B)). However, the χ'' values of MNPs in the lysed MSCs, NHOst cells and MG63 cells showed Brownian-related peaks at approximately 10 kHz, which was similar to that of free MNPs, indicating that intracellular MNPs were released from the cells after cell lysis (Fig. 4(E)).
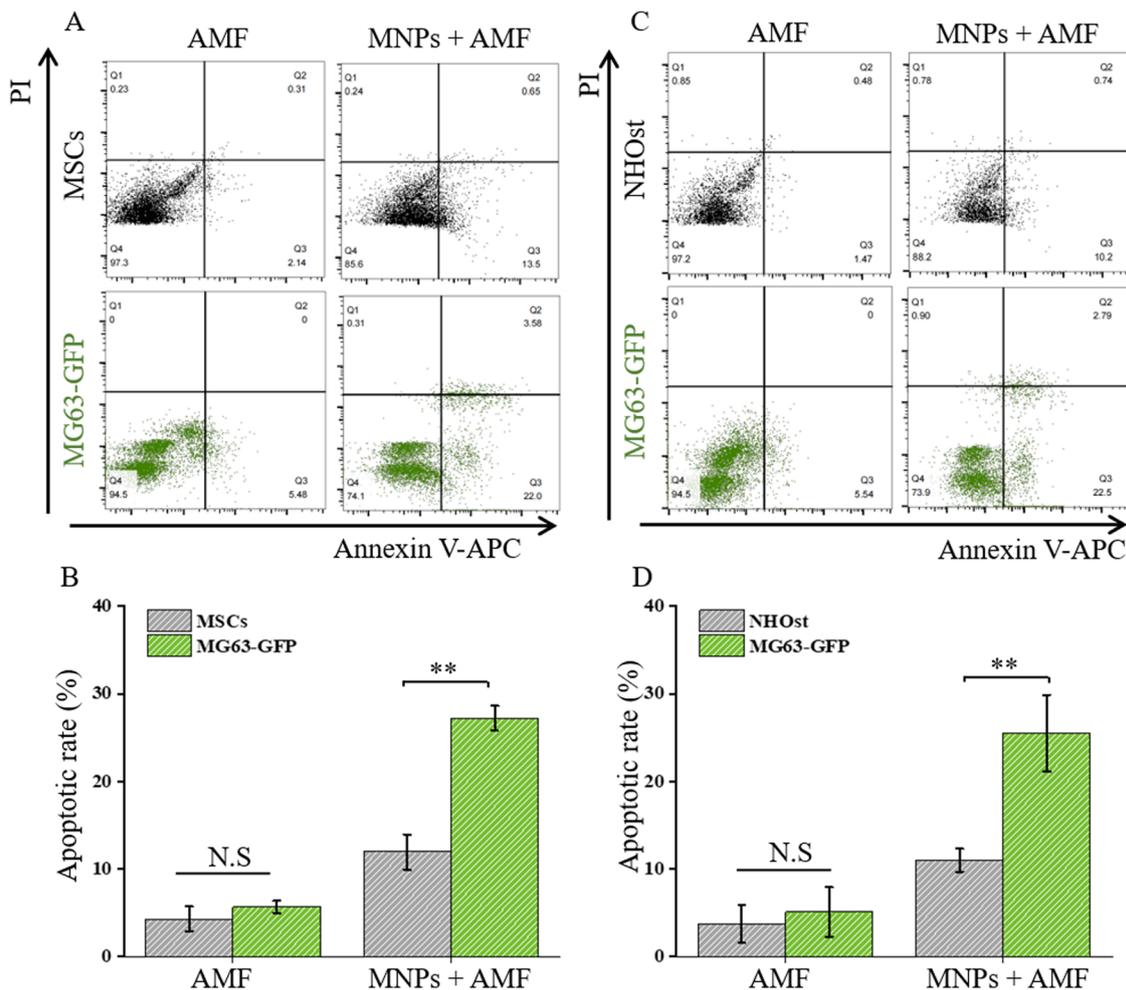
Fig. 3 Apoptosis of cancer cells and normal cells induced by the magnetic hyperthermal effect of MNPs during coculture of MG63-GFP cells and MSCs or NHOst cells. (A) Representative flow cytometry image and (B) apoptosis rate of cocultured MSCs and MG63-GFP cells with or without MNPs after AMF irradiation. (C) Representative flow cytometry image and (D) apoptosis rate of cocultured NHOst and MG63-GFP cells with or without MNPs after AMF irradiation. Data are expressed as the mean ± S.D. (n = 3). Significant difference: **p < 0.01. N.S.: no significant difference.

Simulation of the influence of the intracellular microenvironment on the magnetothermal properties of MNPs using viscous liquids and elastic hydrogels

Cells are active viscoelastic materials whose viscosity and elasticity are dependent on the cell type. Compared with normal cells, cancer cells are less viscous and less elastic due to their disordered cytoskeletal structure.[28–31] The differences in the magnetothermal properties of intercellular MNPs between cancer cells and normal cells are likely related to the differences in viscoelasticity between these cells. To test this hypothesis, viscous liquids and elastic hydrogels were prepared to simulate the viscoelastic properties of living cells to elucidate the influence of viscosity and elasticity on the magnetothermal properties and dynamic magnetic response of MNPs (Fig. 5).

MNPs were suspended in polyethylene glycol (PEG) solutions of different concentrations, and the viscosity increased with increasing PEG concentration (Fig. 5(A), (B) and Table 1). During AMF irradiation, the temperature of the viscous solution increased with increasing irradiation time. However, the rate

of increase in temperature decreased with increasing viscosity (Fig. 5(C)). The SAR of the MNPs also significantly decreased with increasing viscosity (Fig. 5(D)). Moreover, the AC susceptibility of the MNPs was measured, and the results revealed the progressive broadening and shifting of the χ'' peak toward a lower frequency when the viscosity increased (Fig. 5(E)). These results suggested a negative correlation between the Brownian relaxation of MNPs and viscosity.

MNPs were embedded in polyacrylamide (PAAm) hydrogels of different degrees of crosslinking by adjusting the amount of the crosslinking agent N,N-methylenebis acrylamide (Bis). The elastic modulus of the hydrogels increased with increasing degree of crosslinking (Fig. 5(F), (G) and Table 2). Under AMF irradiation, the temperature of the hydrogels increased with increasing irradiation time, and the rate of increase in temperature decreased with increasing hydrogel elasticity (Fig. 5(H)). Furthermore, the SAR of the MNPs (Fig. 5(I)) exhibited the same trend as the temperature changed, indicating an inverse relationship with elasticity. The imaginary Brownian peak of the AC
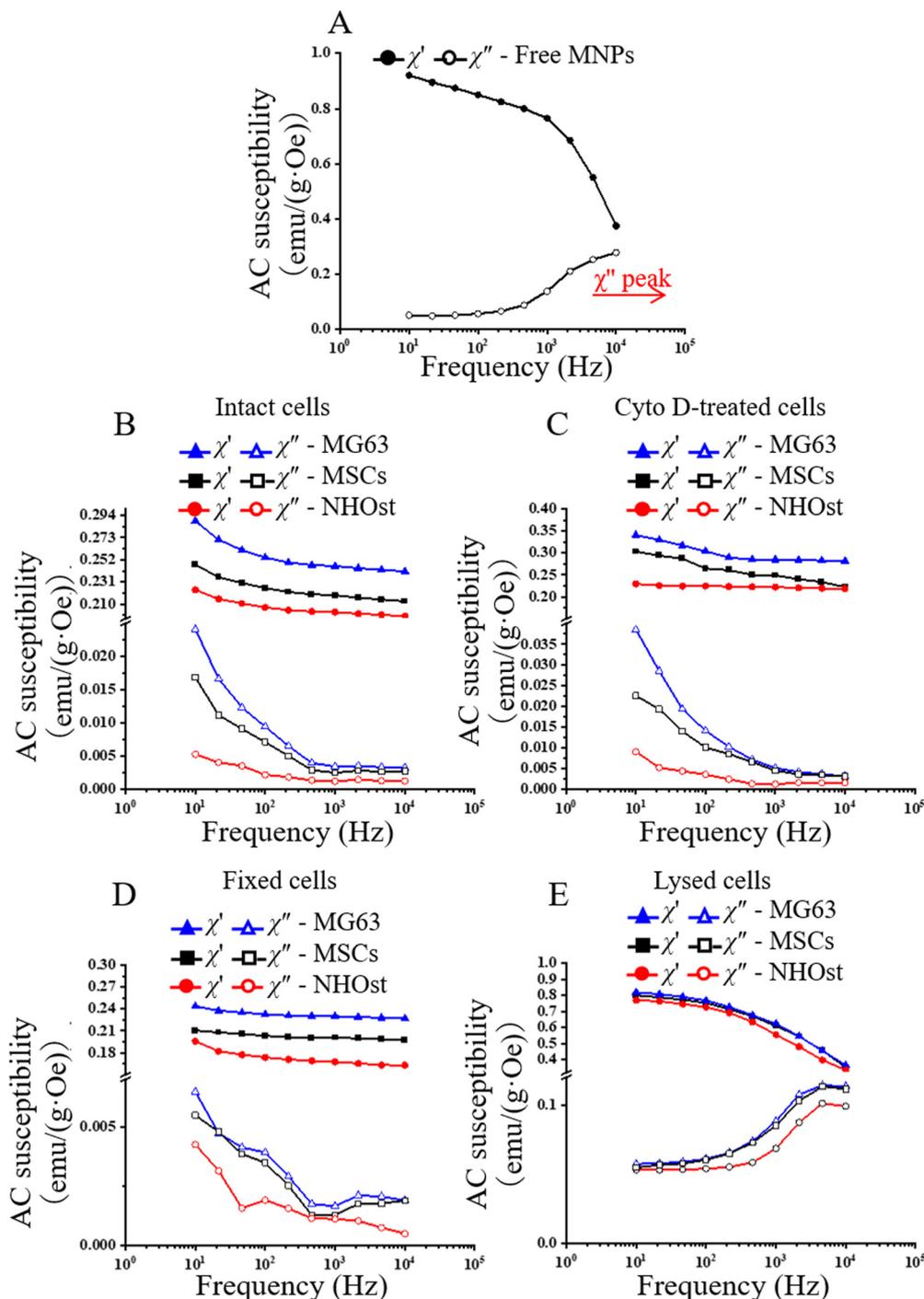
Fig. 4 Comparison of the AC susceptibility of intracellular MNPs in MSCs, NHOst cells and MG63 cells without any treatment or after Cyto D treatment, fixation or lysis. (A) AC susceptibility of free MNPs in water. AC susceptibility of intracellular MNPs in (B) intact cells, (C) Cyto D-treated cells, (D) fixed cells and (E) lysed cells.

susceptibility of the MNPs tended to shift to a lower frequency as the elasticity increased (Fig. 5(J)). Notably, the decreased χ'' values of the MNPs in viscous liquids and elastic hydrogels resembled those of the intracellular MNPs in living cells (Fig. 4(B) and (C)), suggesting that the intracellular microenvironments had similar effects on the dynamic magnetic response of the MNPs via viscosity and elasticity within the cells.

Discussion

Magnetic hyperthermia employs MNPs to create localized heat upon exposure to an AMF. This therapeutic approach has garnered significant attention owing to its excellent biocompatibility and tissue penetration. The European Union has approved Nano-Therm®, an aminosilane-coated Fe_3O_4 superparamagnetic
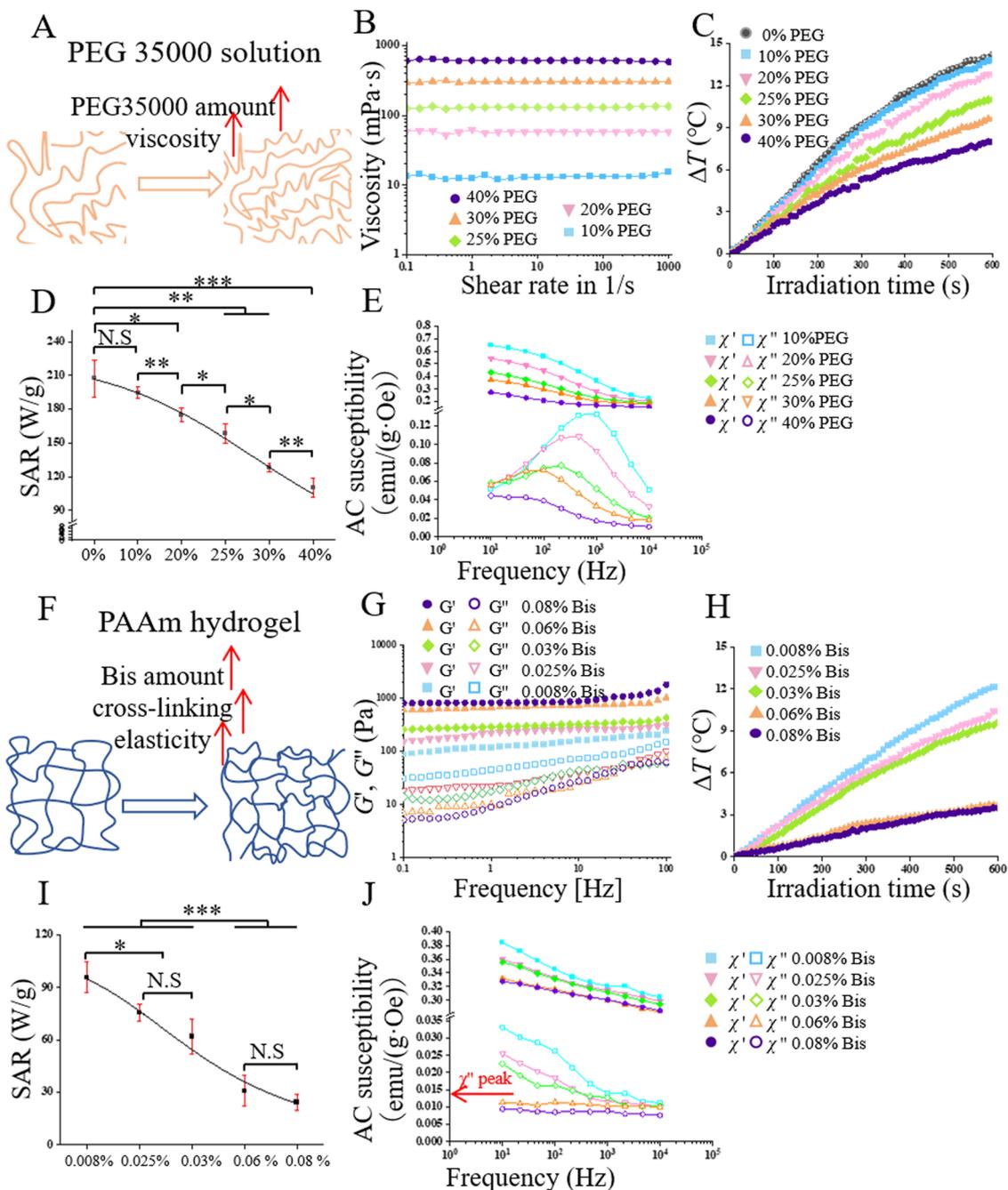
Fig. 5 Influence of the viscosity of liquids and the elasticity of hydrogels on the magnetothermal conversion and AC susceptibility of MNPs. (A) Viscous PEG solutions of different concentrations. (B) Apparent viscosity of viscous PEG solutions at shear rates ranging from 0.1 to 100 s^{-1} at 37 °C. (C) Temperature change, (D) SAR and (E) AC susceptibility of MNPs in viscous PEG solutions under AMF irradiation. (F) PAAm hydrogels with different degrees of crosslinking. (G) Elastic modulus of the PAAm hydrogels. (H) Temperature changes and (I) SAR and (J) AC susceptibility of MNPs in PAAm hydrogels under AMF irradiation. Data are expressed as the mean ± S.D. (n = 3). Significant difference: *$p < 0.05$, **$p < 0.01$, ***$p < 0.001$. N.S.: no significant difference.

Table 1 Viscosity of PEG solutions containing MNPs

PEG solution	10%	20%	25%	30%	40%
Viscosity (mPa s)	13.1 ± 1.2	65.1 ± 7.9	108.6 ± 7.4	290.6 ± 5.3	607.6 ± 27.7

Table 2 Elasticity (G') of PAAm hydrogel embedded with MNPs

PAM hydrogel	8%-Bis 0.008%	8%-Bis 0.025%	8%-Bis 0.03%	8%-Bis 0.06%	8%-Bis 0.08%
G' (KPa)	0.11 ± 0.05	0.27 ± 0.04	0.31 ± 0.03	0.71 ± 0.06	0.89 ± 0.1

nanoparticle, as an adjunctive therapy for glioblastoma in combination with radiotherapy.[36,37] It has been assumed that magnetic hyperthermia for cancer therapy is based on two key factors. One is the enhanced accumulation of MNPs in cancer cells, and the other is poor heat dissipation due to the disorganized and chaotic vascular networks and lymphatic vessels in tumors. However, our study demonstrated that the intracellular microenvironment is also critical for magnetic hyperthermia because the intracellular microenvironment of cancer cells is more favorable for magnetothermal conversion of MNPs than that of normal cells. In other words, the intracellular microenvironment of cancer cells can discriminate the magnetothermal conversion of intracellular MNPs.

The favorable intracellular microenvironment of cancer cells for magnetothermal conversion of intracellular MNPs is likely due to the low viscoelastic properties of cancer cells compared with those of normal cells. This was demonstrated by using Cyto D treatment to soften the cells or by using fixation treatment to stiffen the cells. Both cancer cells and normal cells subjected to Cyto D treatment presented greater magnetothermal conversion of the intracellular MNPs, whereas the fixed cells (both cancer cells and normal cells) presented lower magnetothermal conversion efficiency of the intracellular MNPs than did the untreated cells. A simulation of the viscoelastic intracellular microenvironment using viscous liquids and elastic hydrogels also demonstrated that low viscosity and low elasticity promoted the magnetothermal conversion of MNPs.

Under an AMF, the magnetic moments of MNPs reorient to align with the external field, converting electromagnetic energy into thermal energy. The orientation degree of magnetic moments depends on the properties of the MNPs.[9,38] The superparamagnetic nanoparticles that were used in this study rely on relaxation loss to reorient their magnetic moments for magnetothermal conversion.[39,40] Relaxation includes Néel and Brownian relaxation.[41] Néel relaxation refers to magnetic moment reorientation when MNPs remain immobilized. In contrast, Brownian relaxation refers to entire MNP rotation with reorientation of the magnetic moment.[40] Brownian relaxation converts magnetic energy to thermal energy through the physical rotational friction of MNPs.[42] The intracellular MNPs were not immobilized; thus, the magnetothermal conversion should be based on the Brownian relaxation of the MNPs.

AC susceptibility was utilized to elucidate the influence of the different intracellular environments of cancer cells and normal cells on the Brownian relaxation of MNPs. The χ'' value of the intracellular MNPs in the cancer cells (MG63) was greater and the frequency of the χ'' peak was higher than those in the normal cells (NHOst cells and MSCs) (Fig. 4(B)); this should be due to the less viscous and less elastic intracellular microenvironment of cancer cells, which allows easier rotation of the MNPs compared with the intracellular microenvironment of normal cells. This hypothesis was verified by softening or stiffening the cells or by using models established with different viscous liquids and elastic hydrogels. Softening cells with Cyto D treatment resulted in low viscosity and low elasticity, increasing the χ'' peak frequency of MNPs, while stiffening cells with fixation resulted in high viscosity and high elasticity, decreasing the χ'' peak frequency (ESI,† Fig. S7). Softening the cells, creating lower viscosity and lower elasticity, facilitated easier rotation of the MNPs to generate more heat under AMF irradiation, whereas stiffening the cells, creating higher viscosity and higher elasticity, made rotation of the intracellular MNPs more difficult, generating less heat via Brownian relaxation under AMF irradiation.

The findings of this study suggest that intracellular MNPs could generate more heat to induce more significant apoptosis in cancer cells than in normal cells. The intracellular microenvironment should be considered another critical factor of the magnetic hyperthermal effect of MNPs. These insights provide useful information for optimizing MNP-based hyperthermia to achieve maximal anticancer effects with minimal damage to healthy cells.

Conclusion

The influence of the intracellular microenvironment of cancer cells and normal healthy cells on the magnetothermal properties and magnetic hyperthermal effect of MNPs was elucidated by investigating the magnetothermal conversion, SAR and Brownian relaxation of intracellular MNPs in these cell types. Compared with normal cells (NHOst cells and MSCs), the internalized MNPs in cancer cells (MG63 cells) showed greater temperature changes and SAR values, leading to greater apoptosis rates. These results suggest that the intracellular microenvironment of cancer cells is more conducive to the magnetothermal conversion of MNPs than that of normal healthy cells. The discriminative magnetic hyperthermal effect of MNPs on cancer cells was due to the low viscoelasticity of the cancer cells, which was verified by softening or stiffening the cells and simulated models created using different viscous liquids and elastic hydrogels. The intracellular microenvironment of cancer cells should be considered one of the dominant factors of magnetic hyperthermia.

Materials and methods

Reagents and chemicals

Sodium hydroxide, granular (NaOH), iron(III) chloride hexahydrate ($FeCl_3 \cdot 6H_2O$), iron(II) chloride tetrahydrate ($FeCl_2 \cdot 4H_2O$),

sodium citrate tribasic dihydrate, cytochalasin (Cyto D), Triton X-100, DMEM, Opti-MEM® I reduced serum media, penicillin–streptomycin solution (100×), trypsin-EDTA solution (0.25%), L-glutamine, AAm, Bis, ammonium persulfate (APS) and an annexin V-FITC apoptosis detection kit were purchased from Sigma-Aldrich. Fetal bovine serum (FBS), Alexa Fluor VR 488 phalloidin, Lipofectamine™ 2000 transfection reagent, G418, Geneticin® and eBioscience™ annexin V-APC apoptosis detection kits were acquired from Thermo Fisher Scientific, Inc. A Prussian Blue Stain Kit was purchased from ScyTek Laboratories, Inc. Phosphate-buffered saline (PBS, 10×, pH 7.4) was obtained from Nacalai Tesque, Inc. Hoechst 33258 solution, tetrazolium salt (WST-1 reagent) and a CellStain® double-staining kit were purchased from Dojindo. N-Methyldiethanol-amine (NMDEA), diethylene glycol (DEG), ethanol, ethyl acetate, paraformaldehyde (PFA, 4%), bovine serum albumin (BSA), nitric acid (HNO_3, 67%), hydrogen peroxide (H_2O_2, 30%) and N,N,N',N'-tetramethylethylenediamine (TEMED) were purchased from Wako Pure Industries, Ltd. The pAcGFP1-N1 plasmid expressing GFP was purchased from Clontech Laboratories (Palo Alto, CA). The MSCGM and OBM were purchased from Lonza. All chemicals were used without further purification.

Synthesis and physicochemical characterization of MNPs

MNPs were synthesized *via* a solvothermal method.[43,44] A solution containing 4 mmol $FeCl_3$ and 2 mmol $FeCl_2$ (in polyols of NMDEA and DEG) was stirred for 1 h under an N_2 atmosphere. Afterward, a polyol solution of NaOH was added dropwise to the iron chloride solution and stirred for another 3 h. The mixture was then heated to 220 °C within 1 h. After reacting for 12 h, the black sediment was magnetically separated and washed with a mixture of ethanol and ethyl acetate. The separated black sediment was dispersed in an aqueous solution of sodium citrate and reacted at 60 °C for 24 h to achieve chelation between the MNPs and citrate ions, thereby functionalizing the MNPs with citrate ions. The citrate-MNPs were obtained by centrifugation (12 000 rpm, 15 min) and washed with distilled water three times. The morphology and size of the citrate-MNPs were examined *via* TEM with a JEOL JEM-ARM200F. The XRD patterns and XPS spectra of bare-MNPs and citrate-MNPs were measured by MiniFlex600-Cu and ULVAC-PHI QuanteraSXM, respectively. The FT-IR spectrum of the prepared citrate-MNPs was measured. The normalized field-dependent magnetization (M–H) curve of the citrate-MNPs was measured. The hydrodynamic size and zeta potential of the citrate-MNPs in distilled water or various culture media (DMEM, MSCGM and OBM) was analyzed *via* dynamic light scattering (DLS, Beckman Coulter). Triplicate samples were used for the measurements to calculate the means ± standard deviations.

Biocompatibility of MNPs

The biocompatibility of the MNPs was quantitatively evaluated *via* a WST-1 assay and visualized *via* live/dead staining. The MSCs, NHOst cells and MG63 cells were separately seeded in 96-well cell culture plates at a concentration of 1×10^4 cells per well.

After 24 h, the culture medium was replaced with fresh medium containing MNPs ranging from 0 to 240 μg mL^{-1}, and the cells were cultured for 24 h. After 24 h of culture, the cells were washed with PBS and then incubated in serum-free medium containing calcein AM and propidium iodide (PI) for live/dead staining analysis. In addition, cells treated with various concentrations of MNPs were washed with PBS and incubated with diluted WST-1 reagent for 3 h to assess cell viability. Triplicate samples were used for the measurements to calculate the means ± standard deviations.

Cellular uptake of MNPs

Prussian blue staining was performed to visualize the internalized MNPs in MSCs, NHOst cells and MG63 cells.[45] The three types of cells were cultured in 24-well plates (1.8×10^5 cells per well) and exposed to MNPs at a concentration of 120 μg mL^{-1} for 0–48 h. Then, the cells were washed five times with PBS to remove noninternalized MNPs and fixed. The fixed cells were subsequently incubated with the working iron stain solution for 3 min, followed by three rinses with distilled water and staining of the cell nuclei with nuclear fast red solution for 5 min.[46,47] Finally, the cells were washed and observed under an optical microscope with a bright-field configuration.

ICP-OES was used to quantify the amount of MNPs internalized by MSCs, NHOst cells and MG63 cells. Specifically, each cell type was seeded in a Petri dish (P-100, Falcon) at a concentration of 5×10^6 cells per dish and allowed to adhere for 24 h. Thereafter, the cells were exposed to 120 μg mL^{-1} MNPs for 12 h. After incubation, the cells were rinsed five times with PBS and harvested *via* trypsin/collagenase. The cell suspension was centrifuged (1100 rpm, 5 min), and the collected cells were resuspended in PBS and counted. The collected cells were then digested with 1.0 mL of digestion solution (HNO_3 : H_2O_2, v/v = 2:1) for 1 d. The solutions were subsequently diluted with distilled water and filtered through a 0.22 μm membrane, and the iron content of each sample was determined *via* ICP-OES. Triplicate samples were used for the measurements to calculate the means ± standard deviations.

Influence of the intracellular microenvironment of cancer cells and normal cells on the magnetothermal properties of MNPs

To investigate whether the intracellular microenvironment of MSCs, NHOst cells and MG63 cells affects the magnetothermal properties of MNPs, cells (5×10^6 cells) in Petri dishes (P-100, Falcon) were incubated with 120 μg mL^{-1} MNPs for 12 h. The cells were then rinsed five times with PBS to remove the non-internalized MNPs and obtain MNP-loaded cells. The MNP-loaded cells were used for magnetothermal measurements without any other treatment or after Cyto D treatment, fixation or lysis, as shown below. Triplicate samples were used for the measurements to calculate the means ± standard deviations.

Cells without treatment (intact cells)

MNP-loaded cells were detached with a mixture of trypsin/collagenase solution and then collected *via* centrifugation. Thereafter, the MNP-loaded cells were resuspended in 100 μL

of PBS and transferred into 0.5 mL Eppendorf tubes. The samples were then placed in the center of a Double H CoilSets AMF (frequency: 373.6 kHz; field intensity: 130 Oe) for 10 min (D5 series, nB nanoScale BioMagnetics, Zaragoza, Spain). During AMF irradiation, the temperature of the cell suspension was recorded by a fiber optic thermometer (Rugged Monitoring, Canada).

Cyto D treatment of cells

Actin filaments are the major component of the cytoskeleton and play a key role in regulating cell mechanical properties.[23] Cyto D binds to the actin core and the growth end of F-actin, thereby inducing actin depolymerization and leading to cell softening.[48,49] To investigate whether the cytoskeleton affects the magnetothermal conversion of MNPs, MNP-loaded cells were treated with Cyto D (1.0 μM) for 1 h to disrupt the structure of the actin filaments.[50,51] Then, the cells were detached with a trypsin/collagenase solution, collected *via* centrifugation and resuspended in 100 μL of PBS. The cell suspension was exposed to AMF for magnetothermal measurement.

To investigate the actin filament configuration after Cyto D treatment, Cyto D-treated, MNP-loaded cells were fixed with 4% cold PFA, permeabilized with 0.2% Triton X-100 and blocked with 1% BSA. The actin filaments of the cells were subsequently stained with Alexa Fluor VR 488 phalloidin, and the cell nuclei were stained with Hoechst 33258. The stained cells were observed with a fluorescence microscope (BZ-X710, Olympus).

Fixation of cells

PFA, a widely utilized fixative for cell membranes and cytoplasmic proteins, causes covalent crosslinks between molecules and effectively glues them together to form an insoluble meshwork structure. This process stiffens the cells.[52,53] MNP-loaded cells were detached with a trypsin/collagenase solution, collected *via* centrifugation and resuspended in a mixture of 100 μL of PBS and 900 μL of 4% PFA solution for cell fixation. After 1 h of cell fixation, the fixed cells were washed with PBS three times, collected, dispersed in 100 μL of PBS and exposed to AMF for magnetothermal measurement.

Lysis of cells

MNP-loaded cells were detached with a trypsin/collagenase solution, collected *via* centrifugation and resuspended in 100 μL of PBS. The resulting cell suspension was subsequently lysed *via* five cycles of freezing (liquid nitrogen), thawing (60 °C) and ultrasonic disruption (ice bath). Finally, the lysed cells were exposed to AMF for magnetothermal measurement.

Calculation of the SAR

The magnetothermal conversion efficiency of MNPs in different types of cells without any treatment or after Cyto D treatment, fixation or lysis was quantified by using the SAR.[54] The SAR is the amount of energy converted into heat per unit of time and mass and can be calculated *via* the following equations.

$$\text{SAR} = \frac{1}{m_{\text{MNPs}}} \cdot \frac{Q}{\Delta t} \qquad (1)$$

where Q is the heat (J) generated by the MNPs within a time Δt (s) by a mass (in kg) of MNPs. This is an inherent property of the material.

For an adiabatic system, a calorimetric approach related to the heat dissipated (Q) by MNPs in a colloid and the observed increase in temperature (ΔT) can be calculated *via* eqn (2).

$$Q = (m_{\text{MNPs}} \cdot c_{\text{MNPs}} + m_{\text{cell}} \cdot c_{\text{cell}} + m_{\text{water}} \cdot c_{\text{water}}) \cdot \Delta T \qquad (2)$$

where m_{MNPs}, m_{cell} and m_{water} are the masses of the MNPs, cells and liquid carrier, respectively. The c_{MNPs}, c_{cell} and c_{water} are their specific heat capacities, which are intrinsic characteristics of each material.[55] Therefore, eqn (1) can be written as eqn (3).

$$\text{SAR} = \frac{(m_{\text{MNPs}} \cdot c_{\text{MNPs}} + m_{\text{cells}} \cdot c_{\text{cells}} + m_{\text{water}} \cdot c_{\text{water}})}{m_{\text{MNPs}}} \cdot \frac{\Delta T}{\Delta t} \qquad (3)$$

Since $c_{\text{MNPs}} = 449$ J (K^{-1} kg^{-1}), $c_{\text{cell}} = 4125$ J (K^{-1} kg^{-1}), $c_{\text{water}} = 4185$ J (K^{-1} kg^{-1})[21] and $m_{\text{MNPs}} \cdot c_{\text{MNPs}} + m_{\text{cell}} \cdot c_{\text{cell}} \ll m_{\text{water}} \cdot c_{\text{water}}$, eqn (3) can be written as eqn (4).

$$\text{SAR} = \frac{(m_{\text{water}} \cdot c_{\text{water}})}{m_{\text{MNPs}}} \cdot \frac{\Delta T}{\Delta t} \qquad (4)$$

where $\Delta T/\Delta t$ is the temperature increase (slope) at an early time ($t = 60$ s) during AMF irradiation.

Magnetic hyperthermal of MNPs on cancer cells and normal cells

The apoptotic cells after AMF irradiation were analyzed to evaluate the magnetic hyperthermal effect of MNPs on cancer cells and normal cells. The MSCs, NHOst cells and MG63 cells in Petri dishes (5 × 10^6 cells per dish) were incubated with 120 μg mL^{-1} MNPs for 12 h. The cells were then rinsed five times with PBS to remove the noninternalized MNPs and obtain MNP-loaded cells. Cells cultured without MNPs were used as controls. Some MNP-loaded cells and cells without MNPs were treated with Cyto D to investigate the influence of Cyto D treatment on magnetic hyperthermia. The cells were then detached with a trypsin/collagenase solution and collected *via* centrifugation. Thereafter, the cells in the different groups were resuspended in 100 μL of PBS and transferred into 0.5 mL Eppendorf tubes. The samples were then exposed to AMF (frequency: 373.6 kHz; field intensity: 130 Oe) for 10 min.

After AMF irradiation, the cells were spun down by centrifugation at 1100 rpm and resuspended in 1 × binding buffer. 5 μL of the annexin V-FITC conjugate and 10 μL of PI were added to each tube and incubated at room temperature in the dark for 10 min to stain the apoptotic cells. After passing through a 35 μm nylon filter cover, the stained cell suspensions were transferred to plastic 12 × 75 mm test tubes. Cells cultured without MNPs and before AMF irradiation (control) and MNP-loaded cells before AMF irradiation were also stained. The fluorescence of the cells was measured immediately by using a flow cytometer (BD Accuri C6 Plus). Living cells were

not stained with either PI or the annexin V-FITC conjugate. Early apoptotic cells were stained with the annexin V-FITC conjugate alone, while late apoptotic cells were stained with both the annexin V-FITC conjugate and PI. Both early apoptotic cells and late apoptotic cells were used to calculate the apoptosis rate. Triplicate samples were used for the measurements to calculate the means ± standard deviations.

Discriminative magnetic hyperthermal effect of MNPs on cancer cells in mixed cell populations

MG63 cells were labeled with GFP by transfection with a GFP-encoding plasmid to differentiate cancer cells from normal cells. Normal cells (MSCs or NHOst cells) and cancer cells (MG63-GFP) were cocultured in a Petri dish at a 1 : 1 ratio with a total number of 5×10^6 cells in the presence of 120 μg mL^{-1} MNPs for 12 h. The cells were then rinsed five times with PBS to remove the noninternalized MNPs and obtain MNP-loaded cells. Cocultured cells without MNPs were used as a control. After 12 h of culture with or without MNPs, the cells were collected and exposed to AMF as described above. The apoptotic cells in the mixed cell populations were analyzed by staining and flow cytometry as described above. Normal cells and cancer cells were divided according to green fluorescence. Triplicate samples were used for the measurements to calculate the means ± standard deviations.

AC susceptibility measurement

AC susceptibility is a measure of a material's response to an external magnetic field.[56–58] During AC magnetic susceptibility measurement, the applied magnetic field oscillates between positive and negative values at a set frequency. As the oscillation frequency increases, the magnetic spin of MNPs can irreversibly lag behind the magnetic field switching;[59] this means that while the oscillation frequency of the magnetic spin is the same as that of the external AC magnetic field, there is a phase difference between them. Thus, the AC magnetic susceptibility measurement yields two quantities: the magnitude of the susceptibility, χ, and the phase shift, ϕ (relative to the external AC magnetic signal). Alternately, one can consider susceptibility as having a real AC susceptibility component, χ', and an imaginary component, χ''. The two representations are related by eqn (5) and (6).

$$\chi' = \chi \cos \varphi; \ \chi'' = \chi \sin \varphi \quad (5)$$

$$\varphi = \arctan(\chi''/\chi') \quad (6)$$

The imaginary component, χ'', indicates the Brownian and Néel relaxation dissipation of the MNPs; χ'' will have a nonzero value if there is any lag of the spin behind the oscillating field. To elucidate the relaxation mechanism of intracellular MNPs, the MNPs in different types of cells without any treatment or after Cyto D treatment, fixation or lysis were sealed within tubes (Φ 6 mm, H 40 mm).[60] AC susceptibility measurement was conducted with a magnetometer (Physical Properties Measurement Systems, Quantum Design) at an applied magnetic field

AC amplitude of 10 Oe at room temperature over a frequency range of 10 Hz–10 kHz.[61]

Measurement of the magnetothermal properties of MNPs in simulated models created using viscous liquids and elastic hydrogels

Owing to the cytoskeletal network and high water content of cells, which confers liquid- and solid-like behavior, cells are considered to be multiscale, three-dimensional viscoelastic materials.[62–64] To investigate whether viscosity and elasticity affect the magnetothermal properties of MNPs, PEG solutions of different viscosities and PAAm hydrogels of different elasticities were prepared for comparison. MNPs were suspended in different PEG solutions prepared according to the compositions shown in ESI,† Table S1. The viscosity of the PEG solutions containing MNPs was measured by a rheometer (Anton Parr, Germany) in rotational shear mode.[65] Measurements were conducted with shear rates ranging from 0.1 to 100 s^{-1}, and the viscosity at a shear rate of 0.1 s^{-1} was determined to be the zero-shear viscosity.

Chemically crosslinked PAAm hydrogels were synthesized *via* free radical polymerization of AAm with Bis, and the degree of crosslinking was adjusted by varying the amount of the crosslinker Bis.[66,67] The synthesis conditions are shown in ESI,† Table S2. MNPs were embedded in PAAm hydrogels. Dynamic rheological testing of the PAAm hydrogels containing MNPs was performed with a rheometer. All samples were tested in the linear viscoelastic region, and dynamic frequency sweeps were performed at angular velocities ranging from 0.01 to 100 Hz.[68] All rheological measurements were performed in triplicate at 25 °C.

The viscous solutions and elastic hydrogels containing MNPs were exposed to AMF for 10 min to measure the magnetothermal properties of the MNPs. The SAR values of the viscous liquids and elastic hydrogels were calculated on the basis of the temperature rise (slope) at an early time (t = 60 s) as described above. In addition, the AC susceptibility of the MNPs in viscous solutions and elastic hydrogels was also measured *via* the same method described above.

Statistical analysis

All quantitative experiments were repeated in triplicate (n = 3), and the results are expressed as the mean ± standard deviation (S.D.). Statistical analysis of the experimental data was performed *via* one-way analysis of variance (ANOVA). A p value of 0.05 was set as the level of significance, and data were classified according to their p values as follows: *$p < 0.05$, **$p < 0.01$ and ***$p < 0.001$.

Author contributions

Conceptualization: G. C., M. W., Y. Y. Funding acquisition: G. C., N. K. Project administration: G. C. Resources: G. C. Supervision: G. C. Date curation: G. C., M. W., N. K. Formal analysis: G. C., M. W., R. S., H. C., T. Y., Investigation: G. C.,

M. W., R. S., H. C., T. Y., M. H., M. T. Methodology: G. C., M. W., R. S., H. C., T. Y., N. K., Y. Y. Validation: G. C., M. W., N. K. Software: M. W., N. K., Visualization: M. W. Writing – original draft: All coauthors contributed to original draft. Writing – review and editing: All coauthors contributed to reviewing and editing.

Data availability

The data that support the findings of this study are available on request from the corresponding author.

Conflicts of interest

The authors declare no competing interests.

Acknowledgements

References

1 X. Ma, et al., Modular-designed engineered bacteria for precision tumor immunotherapy via spatiotemporal manipulation by magnetic field, Nat. Commun., 2023, 14, 1606.

2 H. Gavilán, G. M. R. Rizzo, N. Silvestri, B. T. Mai and T. Pellegrino, Scale-up approach for the preparation of magnetic ferrite nanocubes and other shapes with benchmark performance for magnetic hyperthermia applications, Nat. Protoc., 2023, 18, 783–809.

3 A. Chiu-Lam and C. Rinaldi, Nanoscale Thermal Phenomena in the Vicinity of Magnetic Nanoparticles in Alternating Magnetic Fields, Adv. Funct. Mater., 2016, 26, 3933–3941.

4 S.-A. Hescham, et al., Magnetothermal nanoparticle technology alleviates parkinsonian-like symptoms in mice, Nat. Commun., 2021, 12, 5569.

5 X. Liu, et al., Comprehensive understanding of magnetic hyperthermia for improving antitumor therapeutic efficacy, Theranostics, 2020, 10, 3793–3815.

6 L. Chen, et al., Magnetic targeting combined with active targeting of dual-ligand iron oxide nanoprobes to promote the penetration depth in tumors for effective magnetic resonance imaging and hyperthermia, Acta Biomater., 2019, 96, 491–504.

7 M. Kappes, et al., Superparamagnetic Iron Oxide Nanoparticles for Targeted Cell Seeding: Magnetic Patterning and Magnetic 3D Cell Culture, Adv. Funct. Mater., 2022, 32, 2203672.

8 H. Liu, et al., Biocompatible Iron Oxide Nanoring-Labeled Mesenchymal Stem Cells: An Innovative Magnetothermal Approach for Cell Tracking and Targeted Stroke Therapy, ACS Nano, 2022, 16, 18806–18821.

9 H. Gavilán, et al., Magnetic nanoparticles and clusters for magnetic hyperthermia: optimizing their heat performance

10 F. O. Enane, Y. Saunthararajah and M. Korc, Differentiation therapy and the mechanisms that terminate cancer cell proliferation without harming normal cells, Cell Death Dis., 2018, 9, 912.

11 C. Wilhelm and F. Gazeau, Universal cell labelling with anionic magnetic nanoparticles, Biomaterials, 2008, 29, 3161–3174.

12 J. Liu, et al., Tumor microenvironment-responsive metal nanotherapeutics for breast cancer chemo-/immunotherapy, NPG Asia Mater., 2023, 15, 26.

13 O. K. Kosheleva, T.-C. Lai, N. G. Chen, M. Hsiao and C.-H. Chen, Selective killing of cancer cells by nanoparticle-assisted ultrasound, J. Nanobiotechnol., 2016, 14, 46.

14 L. N. M. Nguyen, et al., The exit of nanoparticles from solid tumours, Nat. Mater., 2023, 22, 1261–1272.

15 J. L. Perry, et al., Mediating Passive Tumor Accumulation through Particle Size, Tumor Type, and Location, Nano Lett., 2017, 17, 2879–2886.

16 X. Yang, et al., Comprehensive multi-omics analysis reveals WEE1 as a synergistic lethal target with hyperthermia through CDK1 super-activation, Nat. Commun., 2024, 15, 2089.

17 J.-H. Lee, et al., Exchange-coupled magnetic nanoparticles for efficient heat induction, Nat. Nanotechnol., 2011, 6, 418–422.

18 G. Song, et al., Carbon-coated FeCo nanoparticles as sensitive magnetic-particle-imaging tracers with photothermal and magnetothermal properties, Nat. Biomed. Eng., 2020, 4, 325–334.

19 Y. Zhang, et al., Genetically engineered magnetic nanocages for cancer magneto-catalytic theranostics, Nat. Commun., 2020, 11, 5421.

20 D. Cabrera, et al., Dynamical Magnetic Response of Iron Oxide Nanoparticles Inside Live Cells, ACS Nano, 2018, 12, 2741–2752.

21 A. Espinosa, et al., Magnetic (Hyper)Thermia or Photothermia? Progressive Comparison of Iron Oxide and Gold Nanoparticles Heating in Water, in Cells, and In Vivo, Adv. Funct. Mater., 2018, 28, 1803660.

22 A. M. Master, et al., Remote Actuation of Magnetic Nanoparticles For Cancer Cell Selective Treatment Through Cytoskeletal Disruption, Sci. Rep., 2016, 6, 33560.

23 X. Wang, et al., Morphological and Mechanical Properties of Osteosarcoma Microenvironment Cells Explored by Atomic Force Microscopy, Anal. Sci., 2016, 32, 1177–1182.

24 A. Fromain, J. E. Perez, A. Van De Walle, Y. Lalatonne and C. Wilhelm, Photothermia at the nanoscale induces ferroptosis via nanoparticle degradation, Nat. Commun., 2023, 14, 4637.

25 R. Sun, et al., Composite Scaffolds of Gelatin and Fe_3O_4 Nanoparticles for Magnetic Hyperthermia-Based Breast Cancer Treatment and Adipose Tissue Regeneration, Adv. Healthcare Mater., 2023, 12, 2202604.

26 A. Rajan, M. Sharma and N. K. Sahu, Assessing magnetic and inductive thermal properties of various surfactants

functionalised Fe_3O_4 nanoparticles for hyperthermia, *Sci. Rep.*, 2020, **10**, 15045.

27 A. Saha, *et al.*, Rapid and selective magnetic separation of uranium in seawater and groundwater using novel phosphoramidate functionalized citrate-Fe_3O_4@Ag nanoparticles, *Talanta*, 2021, **231**, 122372.

28 D. Docheva, *et al.*, Researching into the cellular shape, volume and elasticity of mesenchymal stem cells, osteoblasts and osteosarcoma cells by atomic force microscopy, *J. Cell. Mol. Med.*, 2008, **12**, 537–552.

29 A. N. Ketene, E. M. Schmelz, P. C. Roberts and M. Agah, The effects of cancer progression on the viscoelasticity of ovarian cell cytoskeleton structures, *Nanomedicine*, 2012, **8**, 93–102.

30 A. Calzado-Martín, M. Encinar, J. Tamayo, M. Calleja and A. San Paulo, Effect of Actin Organization on the Stiffness of Living Breast Cancer Cells Revealed by Peak-Force Modulation Atomic Force Microscopy, *ACS Nano*, 2016, **10**, 3365–3374.

31 Y. Nematbakhsh, K. T. Pang and C. T. Lim, Correlating the viscoelasticity of breast cancer cells with their malignancy, *Convergent Sci. Phys. Oncol.*, 2017, **3**, 034003.

32 K. Richter, M. Haslbeck and J. Buchner, The Heat Shock Response: Life on the Verge of Death, *Mol. Cell*, 2010, **40**, 253–266.

33 Y. Gu, *et al.*, Local Temperature Increments and Induced Cell Death in Intracellular Magnetic Hyperthermia, *ACS Nano*, 2023, **17**, 6822–6832.

34 M. A. Kang, *et al.*, Magnetically Induced Brownian Motion of Iron Oxide Nanocages in Alternating Magnetic Fields and Their Application for Efficient siRNA Delivery, *Nano Lett.*, 2022, **22**, 8852–8859.

35 K. Wu, *et al.*, Characterizing Physical Properties of Superparamagnetic Nanoparticles in Liquid Phase Using Brownian Relaxation, *Small*, 2017, **13**, 1604135.

36 X. Chen, *et al.*, An injectable and active hydrogel induces mutually enhanced mild magnetic hyperthermia and ferroptosis, *Biomaterials*, 2023, **298**, 122139.

37 M. Zhao, D. Van Straten, M. L. D. Broekman, V. Préat and R. M. Schiffelers, Nanocarrier-based drug combination therapy for glioblastoma, *Theranostics*, 2020, **10**, 1355–1372.

38 S. Dutz and R. Hergt, Magnetic nanoparticle heating and heat transfer on a microscale: Basic principles, realities and physical limitations of hyperthermia for tumour therapy, *Int. J. Hyperthermia*, 2013, **29**, 790–800.

39 X. Yu, S. Ding, R. Yang, C. Wu and W. Zhang, Research progress on magnetic nanoparticles for magnetic induction hyperthermia of malignant tumor, *Ceram. Int.*, 2021, **47**, 5909–5917.

40 E. Izak-Nau, L. P. Niggemann and R. Göstl, Brownian Relaxation Shakes and Breaks Magnetic Iron Oxide-Polymer Nanocomposites to Release Cargo, *Small*, 2024, **20**, 2304527.

41 S. Ota, *et al.*, Characterization of Microscopic Structures in Living Tumor by In Vivo Measurement of Magnetic Relaxation Time Distribution of Intratumor Magnetic Nanoparticles, *Adv. Mater.*, 2024, **36**, 2404766.

42 X. Liu, Y. Tian and L. Jiang, Manipulating Dispersions of Magnetic Nanoparticles, *Nano Lett.*, 2021, **21**, 2699–2708.

43 R. Di Corato, *et al.*, Magnetic hyperthermia efficiency in the cellular environment for different nanoparticle designs, *Biomaterials*, 2014, **35**, 6400–6411.

44 R. Sun, *et al.*, Smart composite scaffold to synchronize magnetic hyperthermia and chemotherapy for efficient breast cancer therapy, *Biomaterials*, 2024, **307**, 122511.

45 M. Maus, *et al.*, Iron accumulation drives fibrosis, senescence and the senescence-associated secretory phenotype, *Nat. Metab.*, 2023, **5**, 2111–2130.

46 N. Daviu, Y. Portilla, M. Gómez De Cedrón, A. Ramírez De Molina and D. F. Barber, DMSA-coated IONPs trigger oxidative stress, mitochondrial metabolic reprograming and changes in mitochondrial disposition, hindering cell cycle progression of cancer cells, *Biomaterials*, 2024, **304**, 122409.

47 C. Deng, *et al.*, Sophisticated Magneto-Mechanical Actuation Promotes *In Situ* Stem Cell Assembly and Chondrogenesis for Treating Osteoarthritis, *ACS Nano*, 2023, **17**, 21690–21707.

48 X. Wang, *et al.*, A novel decellularized matrix of Wnt signaling-activated osteocytes accelerates the repair of critical-sized parietal bone defects with osteoclastogenesis, angiogenesis, and neurogenesis, *Bioact. Mater.*, 2023, **21**, 110–128.

49 M. S. Salker, *et al.*, LeftyA decreases Actin Polymerization and Stiffness in Human Endometrial Cancer Cells, *Sci. Rep.*, 2016, **6**, 29370.

50 L. Yuan, *et al.*, Reconstruction of dynamic mammary mini gland in vitro for normal physiology and oncogenesis, *Nat. Methods*, 2023, **20**, 2021–2033.

51 S. Connolly, K. McGourty and D. Newport, The influence of cell elastic modulus on inertial positions in Poiseuille microflows, *Biophys. J.*, 2021, **120**, 855–865.

52 X. Li, *et al.*, A high throughput microfluidic system with large ranges of applied pressures for measuring the mechanical properties of single fixed cells and differentiated cells, *Biomicrofluidics*, 2022, **16**, 034102.

53 S.-O. Kim, J. Kim, T. Okajima and N.-J. Cho, Mechanical properties of paraformaldehyde-treated individual cells investigated by atomic force microscopy and scanning ion conductance microscopy, *Nano Convergence*, 2017, **4**, 5.

54 Z. Chen, *et al.*, Aptamer-Dendrimer Functionalized Magnetic Nano-Octahedrons: Theranostic Drug/Gene Delivery Platform for Near-Infrared/Magnetic Resonance Imaging-Guided Magnetochemotherapy, *ACS Nano*, 2021, **15**, 16683–16696.

55 Y. Zhang, *et al.*, Impact of Nanoheater Subcellular Localization on the Antitumor Immune Efficacy of Magnetic Hyperthermia, *Nano Today*, 2024, **56**, 102226.

56 C. Shasha and K. M. Krishnan, Nonequilibrium Dynamics of Magnetic Nanoparticles with Applications in Biomedicine, *Adv. Mater.*, 2021, **33**, 1904131.

57 S. Mugiraneza and A. M. Hallas, Tutorial: a beginner's guide to interpreting magnetic susceptibility data with the Curie–Weiss law, *Commun. Phys.*, 2022, **5**, 95.

58 Y. Meng, *et al.*, Experimental Determination of Magnetic Anisotropy in Exchange-Bias Dysprosium Metallocene Single-Molecule Magnets, *Angew. Chem., Int. Ed.*, 2020, **59**, 13037–13043.

59 E. M. Mozur and R. Seshadri, Methods and Protocols: Practical Magnetic Measurement, *Chem. Mater.*, 2023, **35**, 3450–3463.

60 L. Beola, *et al.*, The Intracellular Number of Magnetic Nanoparticles Modulates the Apoptotic Death Pathway after Magnetic Hyperthermia Treatment, *ACS Appl. Mater. Interfaces*, 2020, **12**, 43474–43487.

61 D. Soukup, S. Moise, E. Céspedes, J. Dobson and N. D. Telling, *In Situ* Measurement of Magnetization Relaxation of Internalized Nanoparticles in Live Cells, *ACS Nano*, 2015, **9**, 231–240.

62 A. S. Kashirina, *et al.*, Monitoring membrane viscosity in differentiating stem cells using BODIPY-based molecular rotors and FLIM, *Sci. Rep.*, 2020, **10**, 14063.

63 F. Jia, *et al.*, The role of titanium surface micromorphology in MG-63 cell motility during osteogenesis, *Sci. Rep.*, 2022, **12**, 9971.

64 J. E. Perez, *Transient cell stiffening triggered by magnetic nanoparticle exposure*, 2021.

65 J. Zheng, *et al.*, 3D culture of bovine articular chondrocytes in viscous medium encapsulated in agarose hydrogels for investigation of viscosity influence on cell functions, *J. Mater. Chem. B*, 2023, **11**, 7424–7434.

66 A. Safronov, *et al.*, Polyacrylamide Ferrogels with Magnetite or Strontium Hexaferrite: Next Step in the Development of Soft Biomimetic Matter for Biosensor Applications, *Sensors*, 2018, **18**, 257.

67 N. Jian, *et al.*, Bioinspired Self-Growing Hydrogels by Harnessing Interfacial Polymerization, *Adv. Mater.*, 2023, **35**, 2210609.

68 Q. He, Y. Huang and S. Wang, Hofmeister Effect-Assisted One Step Fabrication of Ductile and Strong Gelatin Hydrogels, *Adv. Funct. Mater.*, 2018, **28**, 1705069.